




Valley polarization investigation of GeS under high pressure

R. Oliva ^{*,†}, T. Woźniak ^{*}, F. Dybala ^{*}, A. Tołłoczko ^{*}, J. Kopaczek, P. Scharoch, and R. Kudrawiec

*Department of Semiconductor Materials Engineering, Wrocław University of Science and Technology,
Wybrzeże Wyspiańskiego 27, 50–370, Wrocław, Poland*



(Received 26 April 2020; revised manuscript received 28 May 2020; accepted 1 June 2020;
published 19 June 2020)

GeS and its analog compounds exhibit unique properties that combine some of the most desired features of other two-dimensional compounds, such as transition-metal dichalcogenides and graphene. These include high electron mobilities or valley physics that result in strong optical and electronic anisotropy. Here, we present an experimental and theoretical study of the electronic band structure of GeS at high hydrostatic pressures. Polarization-resolved high-pressure photoreflectance measurements allow us to extract the energies, optical dichroic ratios, and pressure coefficients of the direct optical transitions. These findings are discussed in view of first-principles calculations, which predict that nondegenerate states in different valleys can be individually selected through linearly polarized light. Based on this, an assignment of the direct optical transitions to the electronic band structure is provided. Finally, the effect of pressure on the electronic band structure is discussed in terms of orbital composition. These results provide evidence that GeS is a strong candidate for valleytronic applications in nondegenerate systems.

DOI: [10.1103/PhysRevB.101.235205](https://doi.org/10.1103/PhysRevB.101.235205)

I. INTRODUCTION

The discovery of graphene [1] triggered enormous research interest in two-dimensional (2D) compounds, owing to their exotic fundamental properties. Intensive research on 2D materials, such as transition-metal dichalcogenides (TMDs), revealed their remarkable electronic and optical properties. These include strong light-matter coupling [2], large excitonic binding energies, the easiness of producing heterostructures by stacking monolayers held by van der Waals (vdW) forces [3,4], as well as the presence of spin-polarized bands that couple to new degrees of freedom such as degenerate valleys or adjacent layers, even in their bulk form [5,6]. Despite the highly promising properties observed in TMDs for many optoelectronic and spintronic applications, alternative 2D materials with complementary properties are being researched. For example, black phosphorus (BP) exhibits superior high carrier mobilities and a sizable gap that can be tuned by adjusting the number of layers, thus combining the most desired features of TMDs and graphene [7,8]. Also, the group-IV monochalcogenides, which are isostructural to BP, have shown to retain many useful properties of BP, such as high carrier mobilities or strong in-plane optical anisotropy that is believed to arise from rich valley physics. In order to fully exploit this family of 2D materials for developing novel optoelectronic devices, it is crucial to further characterize their optical and electronic properties.

Amongst group-IV monochalcogenides, GeS has received particular interest owing to its high electron mobility (larger than $3000 \text{ cm}^2 \text{ V}^{-1} \text{ s}^{-1}$ in its monolayer form [9]), band-gap

value ($\approx 1.6 \text{ eV}$), low toxicity, and high optical anisotropy. These properties are very desirable for photodetectors [10,11], solar cells [12,13], or light-emitting devices [14]. Despite the vast technological potential, the electronic band structure of GeS is not yet accurately known, in particular an assignment of the optical features is still under research. Early polarization-resolved optical absorption measurements revealed that GeS exhibits two optical transitions, E_0 and E_1 , polarized along the *zigzag* and *armchair* directions, respectively, and tentatively assigned them to either direct and indirect transitions [15–17]. More recently, polarization-resolved modulation spectroscopy measurements such as photoreflectance (PR) [18] or thermoreflectance [12,14] allowed measuring the first two direct transitions, namely E_1 and E_2 , polarized along the *armchair* and *zigzag* directions, respectively. However, these transitions have not yet been unambiguously assigned due to difficulties in band-structure calculations such as those based on density-functional theory (DFT). The results of these calculations are highly sensitive to the particular values of lattice parameters, exchange-correlation functionals, van der Waals corrections, or electron-phonon coupling [19–26]. Hence, in order to provide an accurate description of the electronic band structure of GeS, it is desirable to test the state of the art DFT methods by confrontation with optical measurements under different experimental conditions.

High-pressure (HP) modulation spectroscopy represents a unique tool that allows one to obtain detailed information about the electronic band structure [27]. In particular, HP PR measurements allow one to extract the energies of direct transitions and their pressure dependencies, which can be used as a benchmark to test the calculation methods (such as those based on DFT) on challenging systems such as 2D materials [28,29]. To date, many theoretical works reported the effect of strain and pressure on the fundamental properties of GeS.

*These authors contributed equally to this work.

†robert.oliva.vidal@pwr.edu.pl

These studies revealed that the electronic band structure can be strain tuned for ferroelastic switching applications [30] or the band gap can be reduced under compression [9], followed by a semiconductor to semimetal transition. [31,32] These results were confirmed by high-pressure experimental works, which showed that at high pressure GeS exhibits a structural phase transition followed by a metallization [33]. Despite these studies, the effect of pressure on the electronic band structure has been scarcely investigated. Only high-pressure optical absorption measurements reported the shift of the absorption edge with pressure, but the measured optical features were not assigned to the electronic band structure. [34]

In the present work, we perform high-pressure PR measurements in order to assign the optical transitions to the electronic band structure of GeS. Polarization-resolved measurements performed at different pressures are used to resolve the energetically close E_1 and E_2 direct excitonic transitions, as well as to investigate into the anisotropic properties under compression conditions. These results, combined with first-principles calculations, provide valuable information about the electronic band structure of GeS at both ambient and high-pressure conditions. Finally, the anisotropic optical properties are discussed in terms of valley polarization as defined by the selection rules, and the effect of pressure on the electronic band structure is discussed in the context of bands' orbital composition.

II. METHODS

A. Samples

High-purity (>99.995% confirmed) germanium sulfide samples were synthesized by the chemical vapor deposition method. The samples were commercially obtained from the HQ Graphene company. The excellent crystallinity of the samples was confirmed by x-ray diffraction and energy-dispersive x-ray spectroscopy; details can be found elsewhere [35]. An $\approx 200\text{-}\mu\text{m}$ -thick flake was selected for the high-pressure experiments. A picture of the sample selected for the high-pressure experiments is shown in Fig. 1(a). The sample is mounted on the top of a 5-mm-diameter sapphire window of the high-pressure piston-cylinder cell. The orientation of the sample can be inferred from its elongated shape, since GeS typically cleaves forming rectangles, having the largest side along the zigzag direction (b lattice parameter). The orientation of the sample has been confirmed by polarization-resolved photoreflectance measurements (the polarization direction along sample's long edge is set to 0°). The crystal structure, as represented by the VESTA software, is shown in Fig. 1(b) [36].

B. Computational methods

DFT calculations were performed using Vienna *Ab initio* Simulation Package (VASP) [37]. Atomic electronic structures were represented by projector-augmented waves datasets within the Perdew-Burke-Ernzerhof (PBE) parametrization of generalized gradients approximation to exchange-correlation functional [38,39]. A plane-wave basis cutoff of 550 eV and $4 \times 11 \times 9\Gamma$ -centered k -point grid were found to assure

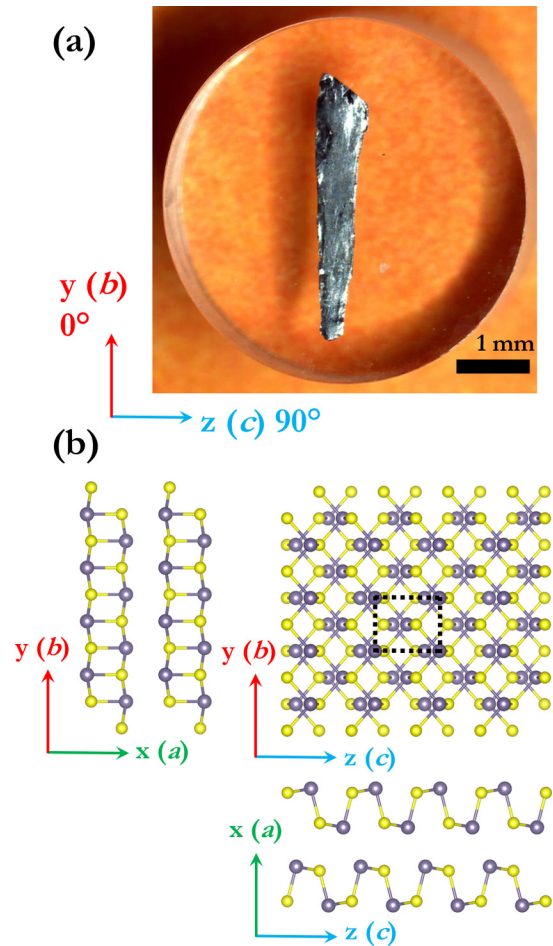


FIG. 1. (a) GeS flake mounted on a sapphire cylindrical window of a piston-cylinder high-pressure cell. GeS flakes typically cleave in rectangular shapes. (b) Representation of the crystal structure of GeS. The armchair and zigzag directions are shown in relation to the crystal orientation and lattice parameters.

convergence of both structural parameters and electronic gaps with precision of 0.001 \AA and 0.01 eV , respectively.

Several methods to represent van der Waals interactions and related functionals were tested to evaluate their effect on the geometry. These are semiempirical corrections: D2 [40], D3 [41], D3 with Becke-Johnson damping (D3+BJ) [42], Tkachenko-Scheffler [43], Tkatchenko-Scheffler with Hirshfeld partitioning (TS+HP), [44] many-body dispersion energy (MBD), [45] dDcS [46], and van der Waals functionals: vdW-DF1 [47] with revPBE, [48] optPBE, optB88, and optB86b [49,50] functionals and vdW-DF2 [51] with rPW86 [52] and B86R [53] functionals. Optimized lattice parameters for all these methods are shown in Table S1 of the Supplemental Material (see Ref. [54] and references therein [55–58]). In the table, calculated lattice parameters are compared to the experimental values. The best agreement is found for the TS, TS+HP, and MBD functionals (corresponding mean absolute relative error, MARE, with respect experimental values is lower than 1%). From the table it is clear that the values of optimized lattice constants, both in plane and out of plane, are sensitive to the vdW method applied. In general, vdW functionals tend to significantly overestimate the lattice

parameters (up to MARE $\approx 6\%$). Therefore the band-structure calculations were performed only for the structures obtained with the semiempirical corrections (see Table S2 in Supplemental Material (SM) [54]). For the present work we used the semiempirical correction of Tkachenko and Scheffler (TS) for vdW interactions for the optimization of lattice constants and atomic positions since it reproduces best the experimental lattice parameters. [43] The geometrical parameters were optimized until all the interatomic forces and isotropic stress were lower than 10^{-3} eV/Å and 0.05 kbar, respectively.

For the electronic band-structure calculations a couple of methods (including local-density approximation, LDA, and PBE exchange-correlation functionals, Heyd-Scuseria-Ernzerhof HSE06 hybrid functional and mBJ-TB09 potential) were tested for all optimized structures as well as for experimental lattice constants (with optimized atomic positions only). Calculated energies with the modified Becke-Johnson exchange potential combined with the LDA correlation (mBJ-TB09) for different optimized structures are shown in Table S2 of the SM. [54] In the present work we conclude that the electronic band structure is best reproduced (in terms of both calculated transition energies and pressure coefficients) by the Tran and Blaha exchange-correlation potential, which consists of the mBJ-TB09 [59]. It is worth noting that qualitatively similar results were obtained with the HSE06 functional (results shown in Table S3 only). The effect of spin-orbit interaction on the lattice parameters and on the transition energies at ambient pressure was lower than 0.001 Å and 0.007 eV, respectively; thus, they were omitted in the high-pressure calculations. The optical matrix elements were obtained from the wave-function derivatives that are calculated within density-functional perturbation theory. [60]

C. Experimental setup

High-pressure hydrostatic measurements were performed by mounting the GeS flake (≈ 4 mm in diameter and ≈ 200 μm thickness) inside a UNIPRESS piston-type cylinder cell. The chosen pressure hydrostatic medium was Daphne 7474, which remained hydrostatic and transparent during the whole experiment, up to a pressure of 18 kbar. The pressure was determined by measuring the resistivity of the InSb gauge by the four-probe method. This method provides a 0.1-kbar sensitivity. A sapphire window guaranteed an optical access to the sample. For the PR measurements, white light from a halogen lamp was focused onto the sample and reflectivity signal was detected by a Si pin diode after the light was dispersed by a 0.55-m focal length single-grating monochromator. Reflectivity on the sample was modulated by a chopped (270 Hz) 405-nm laser line. Phase-sensitivity detection of the PR signal was processed with a lock-in amplifier. A sketch of the whole PR setup is shown in the SM (Fig. S1) [54]. Further details on the experimental setup can be found elsewhere [61].

III. RESULTS AND DISCUSSION

We conducted high-pressure PR measurements in order to determine the pressure dependence of the first direct optical transitions. The PR spectra obtained at different pressures are shown in Fig. 2. As it can be seen in the figure, two PR features

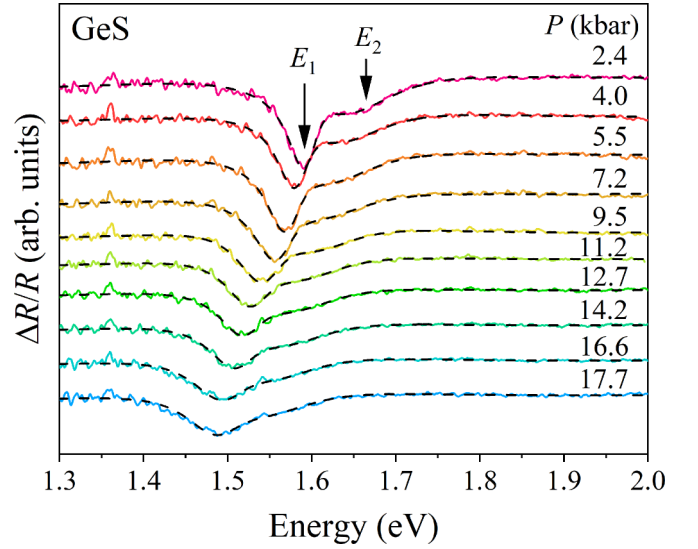


FIG. 2. PR spectra acquired at different pressure values. PR features corresponding to the transitions E_1 and E_2 are shown with labels. Fits to the data are presented as dashed black lines.

show up at $E_1 = 1.61$ eV and $E_2 = 1.66$ eV, whose energies decrease with increasing pressure. These optical transitions have been previously reported from thermoreflectance [12,14] and from polarization-resolved transmittance measurements [17,62]. Calculations predict that GeS is a quasidirect semiconductor with the indirect band gap ≈ 50 meV below the first direct transition (i.e., the indirect transition, not observed in the PR spectra, should be around $E_0 \approx 1.56$ eV at ambient temperature) [26]. To extract the energies of transitions E_1 and E_2 , the PR spectra in Fig. 2 are fitted (dashed lines in the figure) with the Aspnes formula [63],

$$\frac{\Delta R}{R}(\hbar\omega) = \text{Re} \left(\sum C_i e^{i\varphi_i} (\hbar\omega - E_i + i\Gamma_i)^{-m} \right), \quad (1)$$

where C_i , φ_i , Γ_i , and E_i are the resonance amplitude, phase, broadening, and energy of the i th transition ($i = 1, 2$), respectively. These transitions are properly fitted with an excitonic-like resonance profile ($m = 2$), as expected, since the excitonic binding energy is believed to be larger than the thermal energy at room temperature [21]. From the figure it can be seen that, with increasing pressure, both resonances redshift and broaden. At high pressure, both transitions merge, due to an increased pressure coefficient of transition E_2 .

Since the energetic difference between transitions E_1 and E_2 is on the same order of magnitude as their broadening (Γ parameter of the Aspnes formula), polarization-resolved measurements were performed to determine the energies of each transition separately. As can be seen in Fig. 3, the PR profile obtained at 9.4 kbar strongly depends on the polarization angle. At a polarization of 90° (0°) the signal from transition E_1 (E_2) is maximum, which coincides with the direction of the main in-plane lattice parameters c (90° , armchair direction) and b (0° , zigzag direction). This finding is in perfect agreement with previous polarization-resolved absorption [10,12,16,17], thermoreflectance [12,14], and photoluminescence [14,17] measurements, which reported photoluminescence (PL) signal polarized along the armchair direction

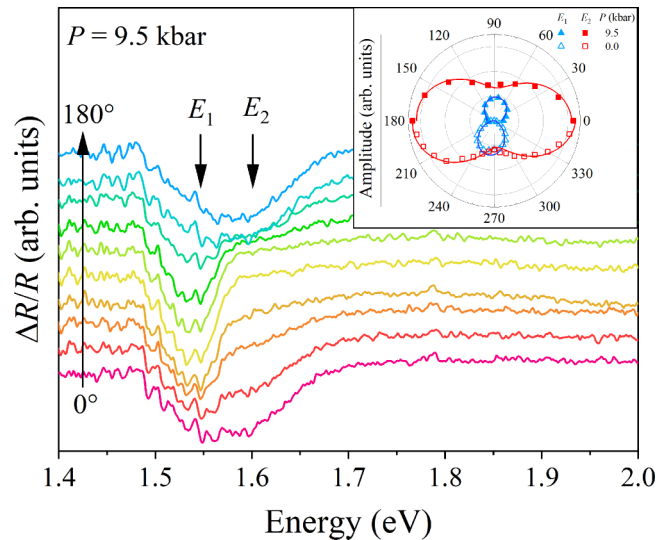


FIG. 3. PR spectra acquired at 9.5 kbar at different polarization directions, from zigzag (0°) to armchair (90°). Inset: Polar plot of the amplitude of transitions E_1 and E_2 at 9.5 kbar (top half) and ambient pressure (bottom half).

at the same energy as the absorption edge measured with the same polarization direction. Thermoreflectance and optical absorption measurements with polarization along the zigzag direction revealed a transition around 50–100 meV higher in energy, which is close to our measured difference of energy ($\Delta E = 49$ meV) between transitions E_1 and E_2 .

The polar dependence of the amplitude (C_i) of each transition is shown in the inset of Fig. 3 for both high pressure (top half of the plot) and ambient pressure (bottom half). As it can be seen in the inset, the amplitudes corresponding to transition E_1 (blue dots) and E_2 (red dots) exhibit maximum at 90° (armchair direction) and 0° (zigzag), respectively. It is worth noting that the fitted amplitude of E_2 is significantly larger than E_1 ; this is due to the fact that the broadening of E_2 is larger than that of transition E_1 . Indeed, the oscillation strength, which is proportional to $|C_i|/\Gamma_i$, is practically identical between both transitions. The polar dependence (solid curves) is fitted by using a modified Malus law,

$$f(\varphi) = f_{\parallel} \cos^2(\varphi - \varphi_0) + f_{\perp} \sin^2(\varphi - \varphi_0), \quad (2)$$

where φ is the light polarization angle, φ_0 is the polarization direction of the transition, and f_{\parallel} and f_{\perp} are the parallel and perpendicular components of the oscillator strength, respectively. While transition E_1 is fully polarized (i.e., $f_{\perp} \approx 0$), the E_2 transition has a significant out of plane component ($f_{\perp} \approx 0.3f_{\parallel}$). The associated optical dichroic anisotropy is around 2000 and 300% for transitions E_1 and E_2 , respectively. These values are on the same order of magnitude as those reported for SnS, around 600% [64]. Here we propose that the decreased optical polarization degree of transition E_2 is caused by parasitic band to band signal from the E_1 transition. Band to band signal is expected as long as the excitonic binding energy of E_1 has a value similar to the ambient thermal energy, around $k_B T_{amb} = 25$ meV. While no excitonic binding energies have been reported so far for bulk GeS, an excitonic binding energy around 30 meV would

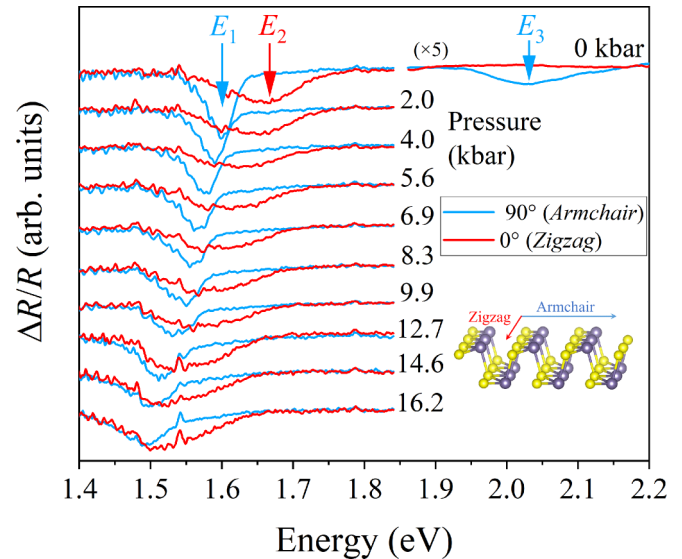


FIG. 4. PR spectra acquired at different pressures with light polarized along the two main crystallographic directions; zigzag (red line) and armchair (blue line). The crystal structure of a GeS layer is shown at the right bottom.

result in some band to band PR signal around the energy of transition E_2 , which is just 49 meV above transition E_1 , but with a perpendicular polarization direction, hence resulting in $f_{\perp} > 0$ for the current fit, as experimentally observed. More work is desirable to clarify the excitonic binding energies of transitions E_1 and E_2 .

In order to individually track the pressure dependence of each optical transition, high-pressure PR measurements with polarizations along the armchair and zigzag directions were performed during the downstroke pressure cycle. The obtained spectra are shown in Fig. 4, where it can be seen that, by using the armchair polarization, two transitions are fully visible. These are E_1 and E_3 (the latter measured at ambient pressure only, due to lack of signal), while transition E_2 shows up only when the zigzag polarization is used. At ambient pressure these transitions are located at 1.61, 1.66, and 1.96 eV, in perfect agreement with previously reported polarization-resolved thermoreflectance measurements that established their energies at 1.59, 1.67, and 2.06 eV, respectively [12]. From Fig. 4 it is clear that the energy difference between transition E_1 and E_2 becomes smaller with increasing pressure. This is due to the increased pressure coefficient of transition E_2 , as discussed below.

Fitted energies by using the Aspnes formula during both the upstroke and downstroke are shown as a functions of pressure in Fig. 5. As it can be seen in the figure, good agreement is found between upstroke (full symbols) and downstroke (open symbols) cycles. For the fitting procedure, the phase and broadening parameters (φ_i , Γ_i) were set at fixed values extracted from fits to polarized spectra at room pressure, and only the amplitude and transition energy parameters (C_i , E_i) were left as free parameters to fit high-pressure spectra. Within this approach, pressure coefficients were obtained from linear fits to the data; dE/dP (meV/kbar) = $-6.9(2)$ and $-8.3(9)$ for transitions E_1 and E_2 , respectively. The

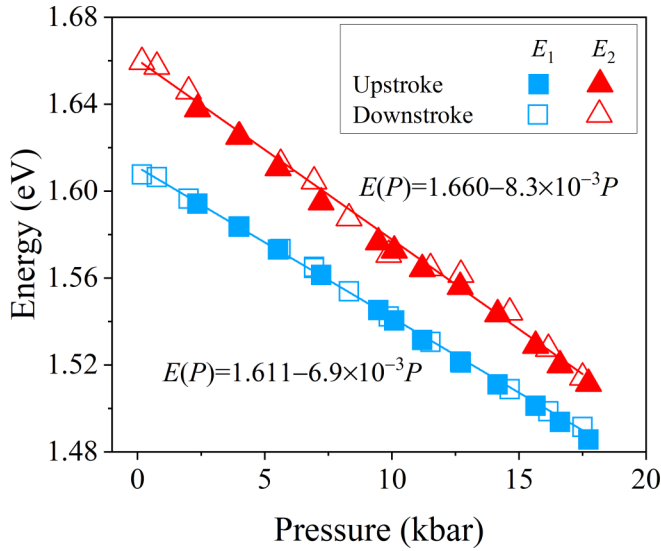


FIG. 5. Pressure dependence of the fitted direct transitions E_1 (squares) and E_2 (triangles) for spectra acquired during the upstroke (full symbols) and downstroke (open symbols) pressure cycles. Linear fits to the data are used to extract the pressure coefficients.

pressure coefficients obtained here are in good agreement with the values from optical absorption measurements reported previously, around -6.0 ± 1.5 meV/kbar for the absorption edge measured under armchair polarization direction (corresponding to the direct transition E_1) and -9.0 ± 1.5 meV/kbar measured under zigzag polarization direction (corresponding to signal arising from both the indirect transition E_0 and the direct transition E_2) [34]. From these results, energetic degeneracy of transitions E_1 and E_2 is expected to take place around 35 kbar. Since the pressure coefficients of transitions E_1 and E_2 are different, it is easier to assign them to the electronic band structure calculated at different pressures.

The calculated electronic band structure is shown in Fig. 6 for zero pressure (black lines) and 20 kbar (gray lines). These calculations predict that the indirect gap (shown as a green arrow) takes place from the valence-band maximum (VBM) close to the Z k -point to the conduction-band minimum (CBM) located around $2/3$ of Γ - Y (labeled as Δ in the figure). The first three direct transitions are labeled E_1 , E_2 , and E_3 and take place at Γ , Δ , and close to Z , respectively. The two latter, which take place at non-high-symmetry k points with an enhanced joint density of states, are band-nesting transitions. These types of transitions have been previously reported in other families of layered compounds such as TMDs [65,66]. More importantly, the electronic band structure shown in Fig. 6 is composed of three valleys, one at Γ and two in the Γ - Z and Γ - Y reciprocal directions corresponding to the armchair and zigzag perpendicular crystallographic directions, respectively. Analog compounds such as SnS, SnSe, and GeSe exhibit a similar electronic dispersion but with a decreased band gap [67]. Interestingly, the two lowest transitions of these compounds in their monolayer form take place only around Z and Δ , while for GeS, a valley at Γ persists even in its monolayer form [68].

It can be shown that the three nondegenerate valleys of GeS can be individually selected by using linearly polarized

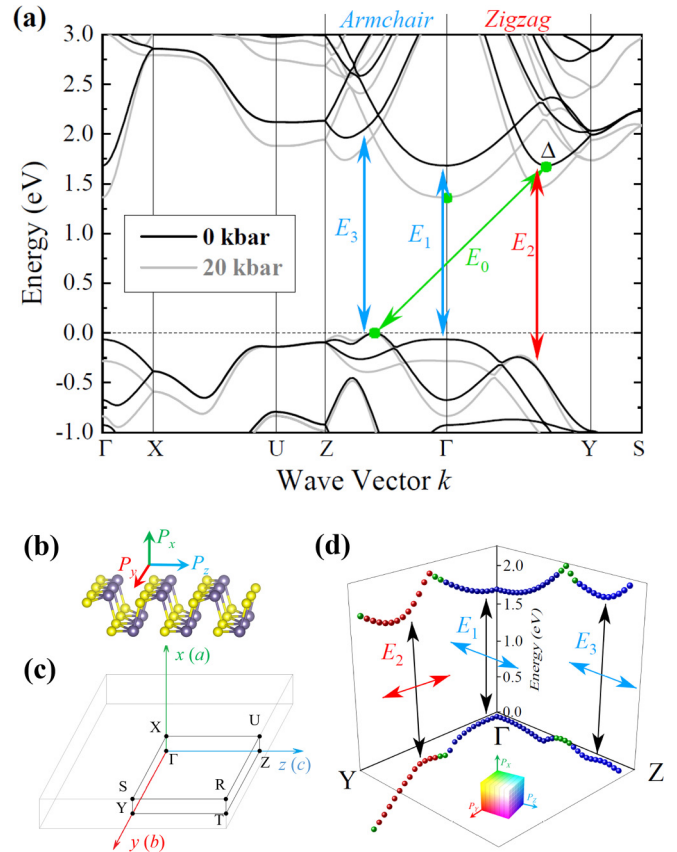


FIG. 6. (a) Electronic band structure calculated along the main high-symmetry points of the Brillouin zone at a pressure of 0 kbar (black curves) and 20 kbar (gray curves). The proposed indirect E_0 transition is indicated (green arrow) as well as the direct transitions E_1 , E_2 , and E_3 (blue and red arrows). CBM and VBM are indicated with green dots. (b) Light polarization directions as defined with respect to the crystal lattice. (c) Brillouin zone with labeled high-symmetry k points. The directions of the lattice parameters are included for clarity. (d) 3D plot of the electronic band-structure lines from (a) in the Y - Γ - Z region of the Brillouin zone. Three valleys are shown to have different polarization directions. For each valley, the matrix elements are shown as a RGB color code (P_y , P_x , and P_z , respectively).

light as a consequence of the selection rules of the crystal $Pnma - D_{2h}^{16}$ space group [69]. This feature can be exploited in designing a variety of valleytronic devices; for instance, transverse nonlinear conductivity has been demonstrated for the SnS analog [70]. In order to investigate the valley polarizability in GeS, optical matrix elements have been calculated along the Y - Γ - Z k -path. Results are shown as a color map in Fig. 6(d) where matrix elements contributing to the directions x , y , and z are represented by colors green, red, and blue, respectively. Our calculations reveal that all transitions are practically fully polarized (i.e., the matrix element for the perpendicular direction is zero), in good agreement with our experiments, which found small or negligible out of plane components of the PR signal (i.e., $f_{\perp}/f_{\parallel} < 0.3$, as previously discussed). It is worth noting that calculated matrix elements within the present method have shown to accurately reproduce the relative photoluminescence intensity of TMDs [71], and

TABLE I. Assignment of direct optical transitions to different points of the BZ. Their respective experimental and calculated energies, polarization directions, and relative pressure coefficients are given.

Transition	Assignment	Energy (eV)		Polarization		$(1/E)dE/dP$ (10^{-3}kbar^{-1})	
		Experiment	Calc.	Experiment	Calc.	Experiment	Calc.
E_1	Γ	1.61	1.68	Armchair	Armchair	-4.3(1)	-3.1
E_2	Δ	1.66	2.05	Zigzag	Zigzag	-5.0(5)	-6.9
E_3	$\approx Z$	1.96	2.06	Armchair	Armchair		-6.6

are in perfect agreement with $\mathbf{k}\cdot\mathbf{p}$ theory for the selection rules of the $Pnma$ space group [70].

The here proposed assignment of the direct excitonic transitions E_1 , E_2 and E_3 to Brillouin-zone (BZ) points is summarized in Table I and has been performed considering the following factors; (i) transition energies, (ii) transition polarization directions, and (iii) pressure coefficients. As can be seen in Table I, the agreement between experimental and theoretical polarization directions is excellent. Within present limitations (no thermal or excitonic effects were considered in the calculations), the agreement between experimental and theoretical transition energies E_1 and E_3 is good (thermal and excitonic effects on the optical energy is expected to be smaller than $\Delta E \approx 250$ meV) [14]. The relative pressure coefficients $(1/E)dE/dP$ are qualitatively in good agreement, where the pressure coefficient of transition E_2 is more pronounced. The calculated here pressure coefficients (-16.0 meV/kbar, -5.2 and -14.1 meV/kbar for the E_0 , E_1 , and E_2 transitions, respectively) are similar to those reported by Makinistian and Albanesi [24] from DFT calculations with GW corrections (-13.0 , -4.8 , and -9.5 meV/kbar for the E_0 , E_1 , and E_2 transitions, respectively). At higher pressures, the pressure coefficients decrease, and our calculations predict a transition to a semimetallic state at 130 kbar (see Fig. S3 in the SM) [54]. This result is consistent with high-pressure structural and electrical measurements, which revealed a phase transition at 90 kbar (phase $P21/m$), followed by a metallization around 150–200 kbar. [33]

The presented high-pressure optical results are useful to evaluate the effect of interlayer coupling on the electronic band structure. The orbital composition of the band structure in the Z - Γ - Y region of the BZ is shown in Fig. 7, where it can be seen that Ge (S) atoms contribute mostly to the conduction- (valence-) band states [see Figs. 7(a) and 6(b), respectively]. Calculated electron density isosurfaces associated with k points corresponding to each of the three direct optical transitions are shown in Fig. 7(c) [Fig. 7(d)] for the conduction (valence) band. From the figures, it is clear that the out of plane component (i.e., x direction) of the orbital composition is dominant at Γ . The pressure dependence positions of the states at Γ result from two competing contributions, on the one hand the destabilization of out of plane p_x orbitals as the interlayer distance diminish and on the other hand the stabilization of the p_x orbitals with contraction of in-plane lattice parameters, resulting in a redshift and a blueshift of the states, respectively. This is in perfect agreement with previously reported uniaxial and biaxial strain calculations, which show that under compression the CB exhibits a redshift

around Γ while the VB a blueshift around Z [9,30–32]. Additional calculations under uniaxial strain, both compressive and tensile, on the electronic band structure further support this interpretation (results are shown in Fig. S2 of the SM). Under hydrostatic pressure, an overall redshift of the states at Γ take place. Indeed, our calculations reveal that with increased pressure, the band gap narrows mostly due to a relative increase of the VB around Z and a decrease of the CB at Γ , which becomes the CBM at 20 kbar [CBM and VBM are represented as green dots in Fig. 6(a)]. Moreover, our calculations show that the gap is closed at 130 kbar for a CBM located at Γ and VBM at Z (see Fig. S3 of the SM) [54]. In general, the effect of increased pressure has a similar impact on the band structure as increasing the number of layers, from monolayer to bulk. This trend has been observed for all GeS analogs, where increasing the interlayer interaction from monolayer to bulk results in an overall decrease of the CBM located at Γ and an increase of the VBM at Z [67]. Similar conclusions have been found for other layered compounds such as MoS_2 and ReS_2 [28].

The clear agreement between calculated and experimental polarization directions (all transitions being fully polarized), qualitative agreement on pressure coefficients and transition energies E_1 and E_3 as shown in Table I, allow us to unambiguously assign the first three optical transitions in the Z - Γ - Y region of the BZ. However, the calculated energy of transition E_2 is significantly overestimated. The fact that GeS analogs (i.e., SnS , SnSe , GeSe) clearly exhibit a prominent valence-band local maxima around Δ , from their monolayer form up to bulk [20,67,68], suggests that calculations fail to reproduce the valence-band electronic dispersion in the Γ - Y region. Similar results are reported in the literature, where most DFT calculations reported decrease [17,20,23,25,26,67] or are inexistent [67,68] VB local maximum around Δ in either bulk or monolayer forms. Angle-resolved photoemission fine-structure spectroscopy measurements show that the local VB at Δ should be ≈ 250 meV below the VBM at Z [72]. From these results, it seems that our calculations underestimate the energy of the VB at Δ by just 150 meV. Since the energetic difference between calculations and experiments is larger (i.e., $\Delta E = 390$ meV, from Table I), we expect that transition E_2 has a large excitonic binding energy, around 240 meV. Such value could be valid in GeS since, in its monolayer form, excitonic binding energies are as large as 0.7–1.2 eV. [22] However, excitonic binding energies are not yet experimentally established for bulk GeS and more work is desirable both experimentally and theoretically to understand the exact electronic dispersion of the valence band in the Γ - Y region of the BZ.

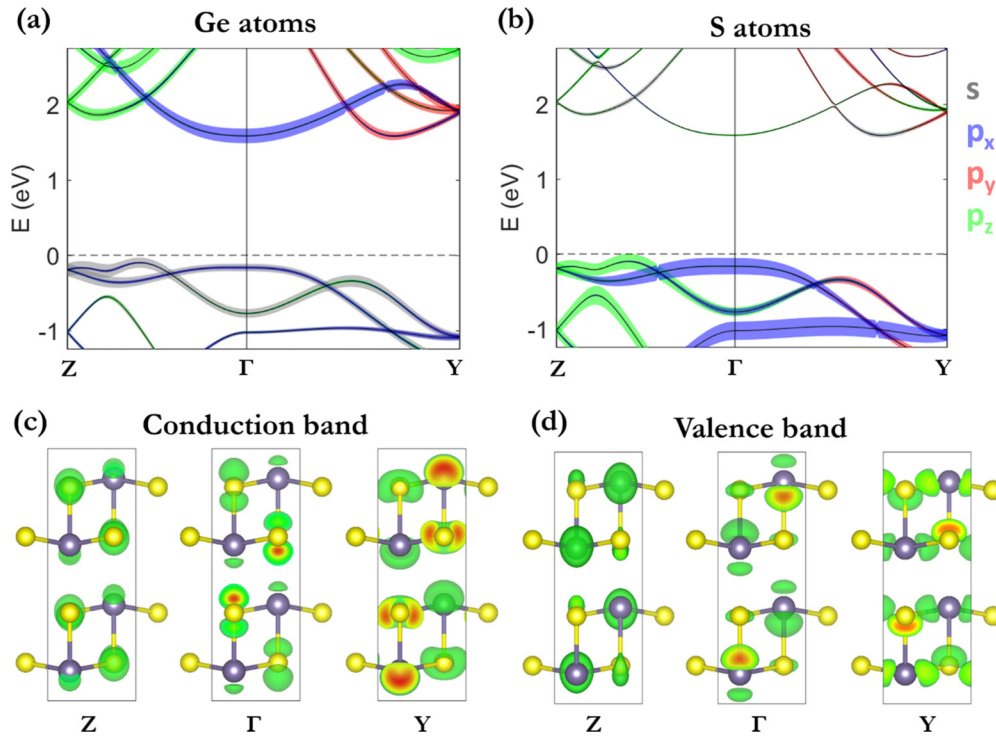


FIG. 7. (a), (b) Calculated band structure in the Z - Γ - Y region of the BZ at zero pressure. The calculated orbital composition for Ge and S atoms (left and right panel, respectively) is represented with different colors (see the legend on the right) and is proportional to the line thickness. Calculations are performed within the PBE functional with TS correction. (c), (d) Plots of calculated electron density isosurfaces (surface level $0.0057 e/\text{\AA}^3$) calculated at k points corresponding to each of the three direct optical transitions (close to the Z , Γ , and Y k points) for conduction-band electrons and valence-band electrons. The view plane is defined by the zigzag- (y) and out of plane (x) directions.

IV. CONCLUSIONS

To summarize, we performed polarization-resolved high-pressure PR measurements on GeS. We found that the first and third direct optical transitions were polarized in the arm-chair direction while the second was polarized in the zigzag direction with dichroic ratios of 2000 and 300%, respectively. Fits to the spectra acquired during the upstroke (unpolarized measurements) and downstroke (polarized measurements) allowed us to extract the pressure dependence of the first two direct optical transitions. The obtained pressure coefficient for the first (second) optical transition is -6.9 meV/kbar (-8.3 meV/kbar). First-principles calculations were used to explore the valley physics in GeS. Calculated matrix elements, transition energies, and pressure coefficients allowed us to unambiguously assign the experimentally measured optical transitions. Finally, the effect of pressure and number of layers on the electronic band structure was discussed in terms of orbital composition. Our results provide a comprehensive

picture of the electronic band structure and optical properties of GeS and validate its potential for valleytronic applications in nondegenerate systems.

ACKNOWLEDGMENTS

This work was supported by the National Science Centre (NCN) Poland OPUS 11 Grant No. 2016/21/B/ST3/00482. R.O.V. acknowledges the support by POLONEZ 3 Grant No. 2016/23/P/ST3/04278. This project is carried out under the POLONEZ program which has received funding from the European Union's Horizon 2020 research and innovation program under the Marie Skłodowska-Curie Grant Agreement No. 665778. T.W. acknowledges support within the "Diamond Grant" No. 0026/DIA/2016/45 from the Polish Ministry of Science and Higher Education. DFT calculations were performed in Wroclaw Centre for Networking and Supercomputing.

- [1] K. S. Novoselov, A. K. Geim, S. V. Morozov, D. Jiang, Y. Zhang, S. V. Dubonos, I. V. Grigorieva, and A. A. Firsov, *Science* **306**, 666 (2004).
 [2] X. Liu, T. Galfsky, Z. Sun, F. Xia, E. Lin, Y.-H. Lee, S. Kéna-Cohen, and V. M. Menon, *Nat. Photonics* **9**, 30 (2015).
 [3] M. Samadi, N. Sarikhani, M. Zirak, H. Zhang, H.-L. Zhang, and A. Z. Moshfegh, *Nanoscale Horiz.* **3**, 90 (2018).

- [4] A. V. Kolobov and J. Tominaga, *Two-Dimensional Transition-Metal Dichalcogenides* (Springer International Publishing, Cham, 2016).
 [5] R. Oliva, T. Wozniak, F. Dybala, J. Kopaczek, P. Scharoch, and R. Kudrawiec, *Mater. Res. Lett.* **8**, 75 (2020).
 [6] X. Zhang, Q. Liu, J.-W. Luo, A. J. Freeman, and A. Zunger, *Nat. Phys.* **10**, 387 (2014).

- [7] A. Castellanos-Gomez, *J. Phys. Chem. Lett.* **6**, 4280 (2015).
- [8] A. Khandelwal, K. Mani, M. H. Karigerasi, and I. Lahiri, *Mater. Sci. Eng.: B* **221**, 17 (2017).
- [9] F. Li, X. Liu, Y. Wang, and Y. Li, *J. Mater. Chem. C* **4**, 2155 (2016).
- [10] Z. Li, Y. Yang, X. Wang, W. Shi, D.-J. Xue, and J.-S. Hu, *ACS Appl. Mater. Interfaces* **11**, 24247 (2019).
- [11] R. K. Ulaganathan, Y.-Y. Lu, C.-J. Kuo, S. R. Tamalampudi, R. Sankar, K. M. Boopathi, A. Anand, K. Yadav, R. J. Mathew, C.-R. Liu, F. C. Chou, and Y.-T. Chen, *Nanoscale* **8**, 2284 (2016).
- [12] H.-C. Hsueh, J.-X. Li, and C.-H. Ho, *Adv. Opt. Mater.* **6**, 1701194 (2018).
- [13] P. Zhao, H. Yang, J. Li, H. Jin, W. Wei, L. Yu, B. Huang, and Y. Dai, *J. Mater. Chem. A* **5**, 24145 (2017).
- [14] C.-H. Ho and J.-X. Li, *Adv. Opt. Mater.* **5**, 1600814 (2017).
- [15] J. D. Wiley, A. Breitschwerdt, and E. Schönherr, *Solid State Commun.* **17**, 355 (1975).
- [16] A. M. Elkorashy, *J. Phys. C: Solid State Phys.* **21**, 2595 (1988).
- [17] D. Tan, H. E. Lim, F. Wang, N. B. Mohamed, S. Mouri, W. Zhang, Y. Miyauchi, M. Ohfuchi, and K. Matsuda, *Nano Res.* **10**, 546 (2017).
- [18] S. J. Zelewski and R. Kudrawiec, *Sci. Rep.* **7**, 15365 (2017).
- [19] A. K. Singh and R. G. Hennig, *Appl. Phys. Lett.* **105**, 042103 (2014).
- [20] B. D. Malone and E. Kaxiras, *Phys. Rev. B* **87**, 245312 (2013).
- [21] L. C. Gomes, P. E. Trevisanutto, A. Carvalho, A. S. Rodin, and A. H. Castro Neto, *Phys. Rev. B* **94**, 155428 (2016).
- [22] B. R. Tuttle, S. M. Alhassan, and S. T. Pantelides, *Phys. Rev. B* **92**, 235405 (2015).
- [23] L. Makinistian and E. A. Albanesi, *Phys. Rev. B* **74**, 045206 (2006).
- [24] L. Makinistian and E. A. Albanesi, *Comput. Mater. Sci.* **50**, 2872 (2011).
- [25] A. Rathor, V. Sharma, N. L. Heda, Y. Sharma, and B. L. Ahuja, *Radiat. Phys. Chem.* **77**, 391 (2008).
- [26] C. E. P. Villegas, A. R. Rocha, and A. Marini, *Phys. Rev. B* **94**, 134306 (2016).
- [27] T. Suski and W. Paul, *High Pressure in Semiconductor Physics I and II, Semiconductors and Semimetals* (Academic Press, San Diego, 1998).
- [28] R. Oliva, M. Laurien, F. Dybala, J. Kopaczek, Y. Quin, S. Tongay, O. Rubel, and R. Kudrawiec, *Npj 2D Mater. Appl.* **3**, 20 (2019).
- [29] F. Dybala, M. P. Polak, J. Kopaczek, P. Scharoch, K. Wu, S. Tongay, and R. Kudrawiec, *Sci. Rep.* **6**, 26663 (2016).
- [30] B. W. Li, Y. Wang, Y. Q. Xie, L. Zhu, and K. L. Yao, *Nanotechnology* **28**, 435202 (2017).
- [31] K. D. Pham, C. V. Nguyen, H. V. Phuc, T. V. Vu, N. V. Hieu, B. D. Hoi, L. C. Nhan, V. Q. Nha, and N. N. Hieu, *Superlattices Microstruct.* **120**, 501 (2018).
- [32] S. Zhang, N. Wang, S. Liu, S. Huang, W. Zhou, B. Cai, M. Xie, Q. Yang, X. Chen, and H. Zeng, *Nanotechnology* **27**, 274001 (2016).
- [33] R. P. Dias, M. Kim, and C.-S. Yoo, *Phys. Rev. B* **93**, 104107 (2016).
- [34] G. Valiukonis, D. A. Guseinova, G. Keivaitb, and A. Sileika, *Phys. Status Solidi B* **135**, 299 (1986).
- [35] GeS - Germanium sulfide, <http://www.hqgraphene.com/GeS.php> (2020).
- [36] K. Momma and F. Izumi, *J Appl Crystallogr.* **44**, 1272 (2011).
- [37] G. Kresse and J. Furthmüller, *Phys. Rev. B* **54**, 11169 (1996).
- [38] G. Kresse and D. Joubert, *Phys. Rev. B* **59**, 1758 (1999).
- [39] J. P. Perdew, K. Burke, and M. Ernzerhof, *Phys. Rev. Lett.* **77**, 3865 (1996).
- [40] S. Grimme, *J. Comput. Chem.* **27**, 1787 (2006).
- [41] S. Grimme, J. Antony, S. Ehrlich, and H. Krieg, *J. Chem. Phys.* **132**, 154104 (2010).
- [42] S. Grimme, S. Ehrlich, and L. Goerigk, *J. Comput. Chem.* **32**, 1456 (2011).
- [43] A. Tkatchenko and M. Scheffler, *Phys. Rev. Lett.* **102**, 073005 (2009).
- [44] T. Bučko, S. Lebègue, J. G. Ángyán, and J. Hafner, *J. Chem. Phys.* **141**, 034114 (2014).
- [45] A. Tkatchenko, R. A. DiStasio, R. Car, and M. Scheffler, *Phys. Rev. Lett.* **108**, 236402 (2012).
- [46] S. N. Steinmann and C. Corminboeuf, *J. Chem. Phys.* **134**, 044117 (2011).
- [47] M. Dion, H. Rydberg, E. Schröder, D. C. Langreth, and B. I. Lundqvist, *Phys. Rev. Lett.* **92**, 246401 (2004).
- [48] Y. Zhang and W. Yang, *Phys. Rev. Lett.* **80**, 890 (1998).
- [49] J. Klimeš, D. R. Bowler, and A. Michaelides, *J. Phys.: Condens. Matter* **22**, 022201 (2009).
- [50] J. Klimeš, D. R. Bowler, and A. Michaelides, *Phys. Rev. B* **83**, 195131 (2011).
- [51] K. Lee, É. D. Murray, L. Kong, B. I. Lundqvist, and D. C. Langreth, *Phys. Rev. B* **82**, 081101(R) (2010).
- [52] É. D. Murray, K. Lee, and D. C. Langreth, *J. Chem. Theory Comput.* **5**, 2754 (2009).
- [53] I. Hamada, *Phys. Rev. B* **89**, 121103(R) (2014).
- [54] See Supplemental Material at <http://link.aps.org/supplemental/10.1103/PhysRevB.101.235205> for the sketch of the experimental setup, electronic bandstructure under strain and higher pressures and tables of calculated lattice parameters and transition energies.
- [55] W. H. Zachariasen, *Phys. Rev.* **40**, 917 (1932).
- [56] G. Bissert and K.-F. Hesse, *Acta Crystallogr. B* **34**, 1322 (1978).
- [57] H. Wiedemeier and H. G. von Schnering, *Z. Kristallogr.* **148**, 295 (1978).
- [58] H. C. Hsueh, M. C. Warren, H. Vass, G. J. Ackland, S. J. Clark, and J. Crain, *Phys. Rev. B: Condens. Matter* **53**, 14806 (1996).
- [59] F. Tran and P. Blaha, *Phys. Rev. Lett.* **102**, 226401 (2009).
- [60] M. Gajdoš, K. Hummer, G. Kresse, J. Furthmüller, and F. Bechstedt, *Phys. Rev. B* **73**, 045112 (2006).
- [61] R. Kudrawiec and J. Misiewicz, *Appl. Surf. Sci.* **253**, 80 (2006).
- [62] F. Lukeš, E. Schmidt, J. Humlíček, and P. Dub, *Phys. Status Solidi B* **122**, 675 (1984).
- [63] D. E. Aspnes, *Surf. Sci.* **37**, 418 (1973).
- [64] S. Lin, A. Carvalho, S. Yan, R. Li, S. Kim, A. Rodin, L. Carvalho, E. M. Chan, X. Wang, A. H. Castro Neto, and J. Yao, *Nat. Commun.* **9**, 1455 (2018).
- [65] A. Carvalho, R. M. Ribeiro, and A. H. Castro Neto, *Phys. Rev. B* **88**, 115205 (2013).
- [66] J. Kopaczek, M. P. Polak, P. Scharoch, K. Wu, B. Chen, S. Tongay, and R. Kudrawiec, *J. Appl. Phys.* **119**, 235705 (2016).

- [67] L. C. Gomes and A. Carvalho, *Phys. Rev. B* **92**, 085406 (2015).
- [68] R. Li, H. Cao, and J. Dong, *Phys. Lett. A* **381**, 3747 (2017).
- [69] M. S. Dresselhaus, G. Dresselhaus, and A. Jorio, *Group Theory: Application to the Physics of Condensed Matter* (Springer-Verlag, Berlin, 2008).
- [70] A. S. Rodin, L. C. Gomes, A. Carvalho, and A. H. Castro Neto, *Phys. Rev. B* **93**, 045431 (2016).
- [71] T. Woźniak, P. E. F. Junior, G. Seifert, A. Chaves and J. Kunstmann, *Phys. Rev. B* **101**, 235408 (2020).
- [72] T. Grandke and L. Ley, *Phys. Rev. B* **16**, 832 (1977).